

A NEW CURVELET-BASED TEXTURE CLASSIFICATION APPROACH FOR LAND COVER RECOGNITION OF SAR SATELLITE IMAGES

Gholamreza Akbarizadeh¹, Zeinab Tirandaz², Monireh Kooshesh³

^{1,2,3} Department of Electrical Engineering, Faculty of Engineering, Shahid Chamran University of Ahvaz, Ahvaz, Iran

Email: ¹g.akbari@scu.ac.ir, ²z.tirandaz@mscstu.scu.ac.ir, ³m.kooshesh@mscstu.scu.ac.ir

Abstract

Texture recognition of synthetic aperture radar (SAR) images, an important technique in the remote sensing area, has been deeply interested in the past decade. It is a key method to analyze this special case of images in practical applications. Watershed transform seems to be a proper method utilized to segment images. However, speckle noise in SAR images and the low resolution of edges make the segmentation and texture recognition difficult in a watershed transformation. Because of excellent results from curvelet transform in feature extraction and filtering as well as watershed advantages in image segmentation, an efficient method to recognize and segment various textures in SAR images is proposed. In this paper, a new algorithm for texture recognition of SAR images is presented. Four main steps in texture recognition of SAR images have been developed in the proposed algorithm. First, the curvelet transform is applied to the SAR image so that the existent image noise is reduced as much as possible. In the second step, the features of various textures in SAR image are extracted based on sub-bands from curvelet transform. In the third step, a label matrix based on the extracted features is formed by the watershed transform. In this matrix, a label is given to a single texture in SAR image which represents watershed regions. Finally, by applying watershed transform to the matrix, the textures of SAR image are classified and recognized. The proposed scheme has been tested on both agricultural and urban SAR images. Experimental results demonstrate the efficiency of the proposed approach in texture recognition of SAR imagery.

Keywords: *Textureclassification, land cover recognition, synthetic aperture radar (SAR) image, and Curvelet transform.*

1.0 INTRODUCTION

Global monitoring for the environment, mapping the earth's resource, recognizing and tracking special objects, and developing military systems require broad-area imaging at high resolutions and acquiring images in inclement weather or during night as well as day [1]. The increasing advancement of research and technology in the field of radar technology has led to the emergence of a new generation of image radars called Synthetic Aperture Radar (SAR). SAR imaging has capabilities to provide broad-area imaging at high resolutions and to acquire images in inclement weather or during night as well as day [2]. SAR systems take advantage of the long-range propagation characteristics of radar signals and the complex information processing capability of modern digital electronics to provide high resolution imagery. Synthetic aperture radar complements photographic and other optical imaging capabilities because of the minimum constraints on time-of-day and atmospheric conditions and because of the unique responses of terrain and targets to radar frequencies [3]. Unique capabilities of radar and SAR images over

optical images resulted in the vast utilization of the images in various applications. These characteristics had a variety of capabilities for radar images in comparison with optical ones: SAR imaging process against optical, is independent from day and night, and weather conditions as well [4]. So, different objects can be identified by texture analysis of the images [5]. However, in addition to the given advantages, the disadvantage is that SAR image processing is highly complicated, and therefore it cannot be definitely said that SAR sensors are able to recognize different objects. In the captured SAR images, objects are seen smaller as well as SAR images are engaged with some noise phenomena called speckle [6]. Image segmentation is considered as an important issue in different fields of image processing and machine vision such as pattern recognition, scene analysis, and image analysis. Image segmentation is the process of dividing images into a variety of regions based on the features like color, texture, and objects present in the images. The regions are sets of pixels which contain useful information regarding the present textures in the image. The result of image segmentation is some form of image whose analysis through the meaningful data becomes easier and more understandable [7]. The different methods presented to segment and recognize SAR image textures, have considered the present noise in SAR images as the main challenge in segmentation [8-10]. A method based on an active contour model by using level set function to segment SAR images proposed in [11]. Active contours are based on two categories: edge-based and region-based. In [12], a local binary fitting (LBF) method has been proposed which was a region-based active contour model. This method extracts the local intensity information from the regions in a controlled scale manner. In this method, two terms were used to control contour movement: one was the edge-based control and the other was ballooned force. The scalability of the LBF method is due to the existence of a kernel function with scale parameters which allows using the local intensity information in a controlled scale value of small neighborhoods. The LBF method does not need the image gradient, which is the main advantage of this method over edge-based active contours. It has also a good performance for weak boundaries images. In [13], region-based methods were used and particular descriptors from every region such as texture, shape, noise and so on have been used to control the movement of the active contour. However, its convergence is faced with the problem. A variety of other methods have been suggested to recognize and classify radar images which function based on the curve evaluation algorithms [14]. In [14], the classical snake method along with several physical noises has been utilized. The principal problem of this method is that the topological changes occur due to the estimation and discretization process of the curve. Segmenting and recognizing new radar image models are all dependent on the homogeneous light intensity in regions which should be segmented. A problem with texture recognition is non-homogeneity of the light intensity distribution in the images. This problem makes the proper recognition of the texture difficult. Non-homogeneous light intensity phenomenon occurs due to the various reasons, among the most effective ones is the noise existent in radar images. In [15], a new region-based active contour model has been proposed to segment SAR images, which makes use of the statistical features of the present pixels in each region of the image. This method is not able to overcome the problem of non-homogeneous light intensity perfectly as well as it is not able to recognize different textures of a SAR image. The present paper suggests an efficient method to segment and recognize SAR images texture by using curvelet method and watershed.

This paper is organized in the following sections. A concise introduction of curvelet and watershed transformation is given in Section 2. Segmentation and recognition of SAR images is illustrated in Section 3. Application of the method and the results are explained in Section 4. ROC curves, AUC of ROC, and accuracy of the proposed method are compared to three other methods in Section 5. Finally, a conclusion is given in Section 6.

2.0 RELATED WORKS

Suppose that we have two functions named $P(x)$ and $Q(y)$ where $x \in (\frac{1}{2}, 2)$ and $y \in [-1, 1]$. The frequency of V_j for each scale $j \geq j_0$, in the frequency domain is defined as [16]

$$V_j(x, \varphi) = 2^{-3j/4} P(2^{-j}x) \cdot Q\left(\frac{2^{\lfloor j/2 \rfloor} \varphi}{2\pi}\right) \quad (1)$$

where $\lfloor \frac{j}{2} \rfloor$ is the integer section of the number $\frac{j}{2}$. If we assume that c_j is the mother curvelet, and $\hat{c}(\omega) = V_j(\omega)$ where V_j is the Fourier transform of c_j . So, the whole curvelets at 2^{-j} can be calculated by translation and rotation of c_j . The angles of rotation are $\varphi_l = 2\pi \cdot 2^{-\lfloor j/2 \rfloor} \cdot l$ where $l=0, 1, \dots$ and $\varphi \leq \varphi_l < 2\pi$ and the translation parameters are defined by $i = (i_1, i_2) \in Z^2$. The curvelets will be defined at scale 2^{-j} , angle φ_L and the position $x_i^{(j,l)} = Y_{\varphi_l}^{-1}(i_1 \cdot 2^{-j}, i_2 \cdot 2^{-j/2})$ as follows [16]

$$c_{j,l,i}(x) = c_j(Y_{\varphi_l}(x - x_i^{(j,l)})) \quad (2)$$

where Y_{φ_L} is rotated by φ_L radians. The curvelet coefficients of a function f are calculated as below [16].

$$k(j, l, i) := \langle f, c_{j,l,i} \rangle = \int_{R^2} f(x) \overline{c_{j,l,i}(x)} dx \quad (3)$$

The curvelet transform can be implemented in the Fourier domain based on Plancherel's theory. In this case, we have [16]

$$\begin{aligned} k(j, l, i) &:= \frac{1}{(2\pi)^2} \int \hat{f}(\omega) \overline{\hat{c}_{j,l,i}(\omega)} d\omega \\ &= \frac{1}{(2\pi)^2} \int \hat{f}(\omega) V_j(R_{\varphi_l} \omega) e^{i\langle x_i^{(j,l)}, \omega \rangle} d\omega \end{aligned} \quad (4)$$

If using Cartesian arrays is considered, then the Cartesian window is given by [16]

$$\tilde{V}_j(\omega) := R_j(\omega_1) Q_j(\omega) \quad (5)$$

where $R_j(\omega_1) = R(2^{-j} \omega_1)$, $R(\omega_1) = \sqrt{c(\omega_1/2)^2 - c(\omega_1)^2}$, and $Q_j(\omega) = Q\left(2^{j/2} \omega_2 / \omega_1\right)$. In this case,

$Q_j(\omega)$ is a set of slopes $\varphi_l = l \cdot 2^{-\lfloor j/2 \rfloor}$ with equal spaces, $l = -2^{-\lfloor j/2 \rfloor}, \dots, 2^{\lfloor j/2 \rfloor} - 1$, and $\varphi_l \in \left[-\frac{\pi}{4}, \frac{\pi}{4}\right]$.

So, we have [16]

$$\tilde{V}_j(\omega) := R_j(\omega_1) Q_j(S_{\varphi_1} \omega). \quad (6)$$

Here, S_{φ_1} is a shear matrix where $S_{\varphi_1} := \begin{pmatrix} 1 & 0 \\ -\tan \varphi_1 & 1 \end{pmatrix}$. $\tilde{U}_{j,l}(\omega)$ window is a concentric tiling, which is shown in Fig.1 [16].

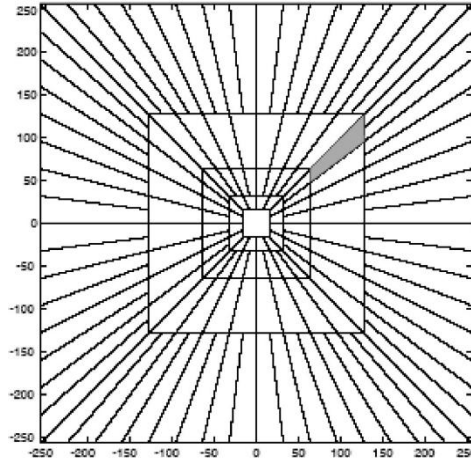


Fig. 1. Curvelet tiling of frequency [16].

Curvelet coefficients are obtained as [16]

$$k(j, l, i) = \int \tilde{f}(\omega) \tilde{U}_j(S_{\varphi_1}^{-1} \omega) e^{i \langle S_{\varphi_1}^{-1} \omega, b \rangle} d\omega. \quad (7)$$

Here, b has discrete values, $b := \left(i_1 \cdot 2^{-j}, i_2 \cdot 2^{-j/2} \right)$ [16].

Candès *et al.* proposed two Fast Discrete Curvelet Transform (FDCT) algorithms, one based on unequally spaced Fast Fourier Transform (FFT) and the other based on wrapping of specially selected Fourier samples [16, 17].

This paper used wrapping because it is more perceivable intuitive and it needs shorter calculation time. “Wrapping” steps are as follows [16]:

- 1- Applying 2-DFFT and obtaining Fourier samples of $\hat{f}[\omega_1, \omega_2]$ where $\omega_1, \omega_2 \in 2\pi Z$ and $-\pi N \leq p_1, p_2 < \pi N$ [16].

2- Forming $\tilde{U}_{j,\varphi_L}[\omega_1, \omega_2]$ and $\hat{f}[\omega_1, \omega_2]$ for each j scale and l angle [16].

3- Putting wrap of the generated function around its origin value and obtaining $\tilde{f}_{j,l}[\omega_1, \omega_2] = P(\tilde{U}_{j,l} \hat{f})[\omega_1, \omega_2]$ [16].

4- Applying reversed form of 2-DFFT for each $\tilde{f}_{j,l}$ and collecting discrete coefficients of $K^D(j, l, i)$ [16].

After FDCT, curvelet coefficients are directly related to the scales and different directions of the original image. High frequencies of noise should be removed to improve the image. The relationship between coefficients should be considered while removing the noise. The high-frequency coefficients were compressed on small scales. In other words, there are low noises with small deviations on a large scale. On different scales, noise deviations almost follow the Gaussian distribution [18, 19]. However, noise deviations are almost equal on even scales at different directions.

Noise deviation estimation on large scales:

$$\sigma^2_{j,l}(l) = e^{1-l^{1.2}}. \quad (8)$$

Noise deviations on fine and detailed scales [18-20]

$$\sigma^2_{j,l}(l) = \frac{\text{Median}(|\omega_{i_1, i_2}|)}{\gamma}. \quad (9)$$

$\sigma \cdot 0.6745$ and ω_{i_1, i_2} are curvelet coefficients on a small scale. $\lambda_{j,k}$ is bigger than noise coefficients, which is defined as [18]

$$\lambda_{j,l} = \frac{\sigma_{j,l}}{\log(j+1)} \sqrt{2 \log N}. \quad (10)$$

Therefore, the modify function is similar to the one mentioned in [18, 21] for the wavelet.

$$\begin{cases} T_{j,l}(x) = 1 & x < k_1 \lambda_{j,l} \\ T_{j,l}(x) = (k \frac{m}{c_2 \lambda_{j,l}})^n & x < k_2 \lambda_{j,l} \\ T_{j,l}(x) = (\frac{m}{x})^n & k_2 \lambda_{j,l} < x < m \\ T_{j,l}(x) = 1 & x > m \end{cases} \quad (11)$$

In Eq. 11, n ($0 < n < 1$) determines rate of nonlinearity. K_1 ($0 < k_1 < 1$) regulates the estimated noise deviation. M_{\max} ($0 < l < 1$) and $m=1$ are selected. M_{\max} is the biggest coefficient in the relative band. If the image is infected with serious noises, the tune value can be set on $T_{j,l}(x) = 0$ for removing the noise [18].

Therefore, the denoising algorithm is shown in Fig. 2 [18].

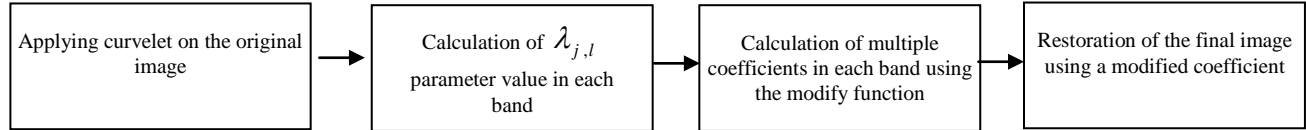


Fig. 2. Schematic diagram of denoising algorithm based on Curvelet transform.

In image processing, the edges are generally in the form of curves and the wavelet and ridgelet transforms are not able to present them efficiently, but in proper scales, a curved edge is transformed into a straight line. On the principle of this method, Candès and Donoho presented another multi-criteria transformation called first generation curvelet to illustrate curved form discontinuities more efficiently [22]. The idea in this method is dividing the curves into a set of small straight lines and processing each piece by ridgelet transformation. Ridgelet transformation matches discontinuities with higher dimensions. One-dimensional discontinuities can be in the form of straight or curved lines. Ridgelets are only matched with straight line discontinuities and are effective for them. Curvelet transformation is a multi-scalar transformation, and presents the structural information in an image based on multi-radius directions in the given frequency range. The main idea of this transformation is analyzing the image into a set of sub-bands and calculating the obtained coefficients to analyze the given texture [23]. Curvelet transform is not limited to spatial and frequency domain. It can also perform in angular detection. Geometric characteristics of constructions have been ignored in wavelet transform. Thus denoising becomes inefficient computationally for features with surface and line irregularities. The first generation of the curvelet transform was implemented for image denoising for the first time by Candès and Guo [24], and by Starck et al. [25] in 2002. In 2004, the second generation of curvelet was proposed by Candès and Donoho. After that the application of curvelets was expanded quickly. Amongst the main applications of the curvelet transformation are the noise removal, improvement, and classification of SAR images. Curvelet transform has been introduced recently as multi-scale transformation which allocates an optimum detection for noise disturbance [25-27]. Ma and Plonka introduced two various algorithms for combining nonlinear diffusion schema with discrete curvelet transform [28]. In this model, a shrinkage curvelet is implemented to the noisy data points and then projected variation diffusion was applied for reducing the Pseudo-Gibbs artifacts. In the second model [29], a nonlinear reaction-diffusion was implemented and then the curvelet shrinkage was applied as a regularizer of the diffusion process. B. Zhang et al. [30] used curvelet for noise reduction and compared it with wavelet and ridgelets. Tessens et al. [31] used curvelet domain statistics for context image denoising. In this method, an inter-subband statistical evaluation of curvelet coefficients was performed that can categorize two classes of coefficients. One is the parts of the image that are useful and the other is the parts that are dominated by noise. In [31], a model based on marginal statistics, which is an appropriate method for indicating local spatial activities, was proposed. This model was very useful for image denoising [32]. Fig. 3 illustrates the complete process of calculating curvelet transformation for an image. In the process, the image that is analyzed into a set of sub-bands is given. Ridgelet transformation is applied to each block in the end.

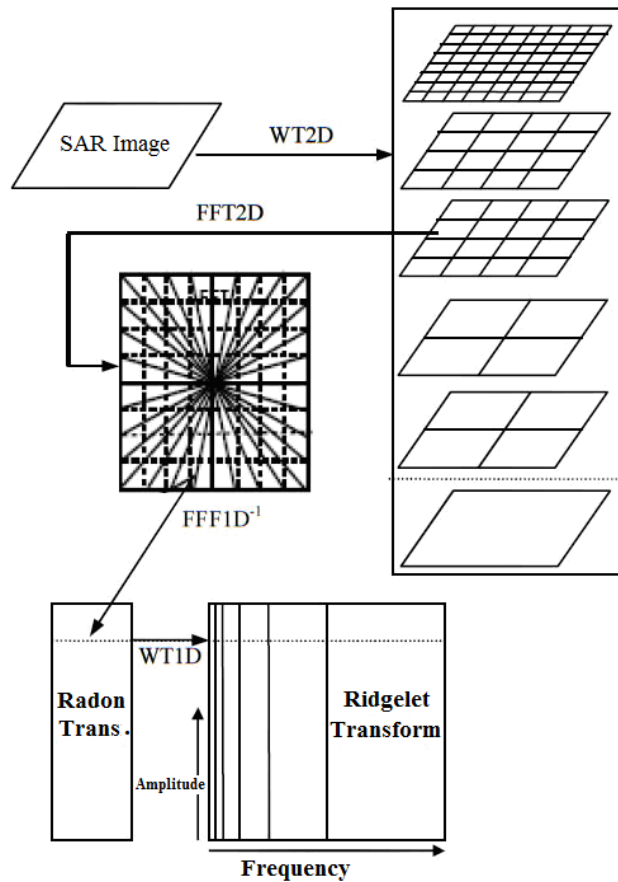


Fig. 3. The complete calculation process of curvelet transform for an image.

The basic definition of watershed is distance-based that follows the theory of topographical distance. It is assumed that watershed is defined for a given relief function $f(x): X \in R$ in some of the domains of $X \subset R^2$.

Definition 1. For every function f , the topographical distance between the two points x and y is the weight of the distance with a gradient norm of $|\nabla f|$ [33]:

$$L(x, y) = \inf_{\gamma \in [x \rightarrow y]} \int_{\gamma} |\nabla f(\gamma(s))| ds. \quad (12)$$

Here, $[x \rightarrow y]$ represents a set of possible paths from x to y . Eq. 12 is applicable when the function is smooth. When the function is not smooth, a discrete version of the Eq. 12 is applied, which was proposed by Meyer [34]:

$$\tilde{L}(x, y) = \min_{\pi} \sum_{i=2}^n \nabla(r_{i-1}, r_i) \text{dist}(r_{i-1}, r_i). \quad (13)$$

Here, $\text{dist}(\cdot)$ represents the Chamfer distance [35]. The minimal path is selected among all of the possible paths from x to y through adjacent pixels $\pi = r_1, r_2, \dots, r_n$. Here, $r_1=x$, $r_n=y$ and r_i and r_{i-1} are equal inside the vicinity of Chamfer. $\nabla(r_{i-1}, r_i)$, approximates the gradient norm. Based on Meyer’s proposed method [34], $\nabla(r_{i-1}, r_i)$ is defined as follows [33]:

$$\nabla(r_{i-1}, r_i) = \begin{cases} LS(r_i) & \text{if } f(r_{i-1}) < f(r_i) \\ LS(r_{i-1}) & \text{if } f(r_{i-1}) > f(r_i) \\ \min\{LS(r_i), LS(r_{i-1})\} & \text{if } f(r_{i-1}) = f(r_i) \end{cases} . \quad (14)$$

Here, $LS(r_i)$ is the lower slope in r_i [33, 34].

Function f has a limited number of regional minima [36], denoted by M_1, \dots, M_p . α_i represents the surface of f over M_i . Eq. 15 is used for topographical distance conversion for the regional minimum [33]:

$$L_i(u) = L(u, M_i) = \inf_{v \in M_i} L(u, v). \quad (15)$$

The p values are obtained for each point inside the regional minima distance. Catchment basins and watershed lines are defined as follows [33]:

Definition2. The catchment basin CB_j , which is located inside regional minimum M_i , is defined as follows [33]:

$$CB_i = \{u \in U \mid \forall j \neq i, 1 \leq j \leq P: \beta_i + L_i(u) < \beta_j + L_j(u)\} . \quad (16)$$

Definition3. In function f , the watershed line is a set of points that do not belong to the catchment basin line [33]:

$$WS(f) = U \setminus \bigcup_i CB(M_i). \quad (17)$$

If regional minima are at the same level, watershed is the SKIZ (skeleton by zones of influence) topography [37] inside regional minima.

The function f can be retrieved from the regional minima distance [34]:

$$f(x) = \min_{1 \leq i \leq K} \{\beta_i + L_i(x)\}. \quad (18)$$

In practice, watershed lines are created from a set of given regions, which are called markers, to avoid oversegmentation. First, all marker points are set to a minimum value such as zero and a new relief is created by recursive conditional erosion [33]:

$$g_{n+1} = \max\{f, \mathcal{E}g_n\}. \quad (19)$$

Here, $g_0(x)$ is a function whose value is 0 on the markers and ∞ otherwise. $\mathcal{E}g_n$ represents the erosion g_n of minimum disk. Next, watershed conversion is applied to g_∞ , which has markers with just a single minimum value.

The classic watershed line in g_∞ is a subset of the watershed line of the original function with the most important holding edges [33].

If s_m is a set of markers, the given path π is from x to s_m . In this case [33]:

$$C(\pi) = \max_{z \in \pi} f(z) \quad (20)$$

$C(\pi)$ is called the connection cost in [38], which is used to recover the relieves. $g_\infty(x)$ can be interpreted as the maximum water level of the markers that must be obtained before flooding of x [33]:

$$g_\infty(x) = \min_{\pi \in [x \rightarrow s_m]} P(\pi). \quad (21)$$

Here, $[u \rightarrow s_m]$ represents a set of paths; therefore, it links x and s_m together.

Watershed transformation is a topological tool for segmenting and dividing an image [7]. Christian Lantueioul [39, 41] studied the effect of a binary accumulation of gains for modeling a polycrystalline alloy. He investigated the geodesic metric that is used for building a SKIZ in [40, 41]. To study the drainage characteristics of a topographic surface, he built minima's geodesic SKIZs. It was the first algorithm of building of watersheds. Lantuejou and Sege Beucher [40, 41] implemented the watershed to segment an image of gas bubbles. It was the first time that watershed had been used for the application of segmentation. In 1997, Diagabel et al. [42] presented the watershed transformation as abased-morphological tools. Then, F.Maisonneuve approached the watershed theoretically, and after that, it has been used in many grayscale segmentation problems. Nowadays, it is being used to study the different points of view, such as theoretical, practical, and algorithmical applications [43]. The watershed segmentation was improved by Li et al. in 2003. They proposed a method that represents watershed segmentation using appearance knowledge and formal shape to improve their methods [44]. Watershed transformation can be considered as a region-based segmentation approach. The segmentation of SAR images into homogeneous and meaningful regions based on Watershed transform is the next step in this paper. Fig. 4 shows an image of the watershed transformation process for different regions. According to this figure, the main idea of watershed appears like a landscape of immersing regions in a lake. Different watershed regions are illustrated with catchment basins (CBs), and each region is filled up with water starting at each local minimum. The discrete lines on the figure represent watershed dams constructed to prevent water from leaking into other basins. As a general result, it

can be seen that the watershed lines have had the efficiency to separate and segment the various regions in the landscape.

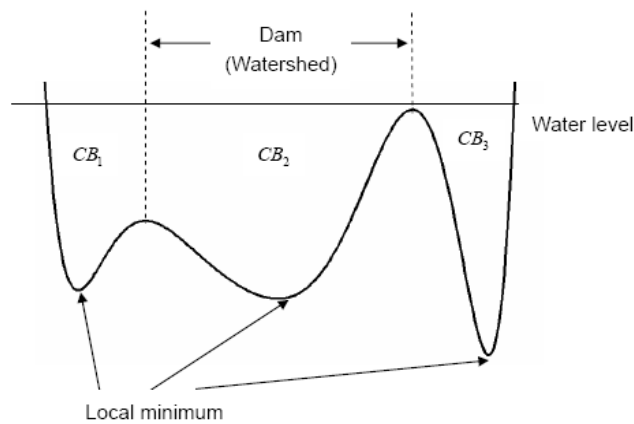


Fig. 4. Watershed transform process for various regions.

Watershed transformation is used as $L = \text{watershed}(A)$ in MATLAB program. A label matrix which determines watershed regions is calculated from the input matrix A . The matrix can be of any dimensions. In the present paper, the input matrix A is a 2 dimensional matrix. The calculated elements of matrix L are integer values which are greater than or equal to zero. These labels are called watershed pixels. In the calculated matrix L , the labeled elements 1 belong to the first watershed region, and 2 belong to the second one. The process continues for other regions as well. The labeled elements zero in the matrix L characterize the borders between the various regions. Amongst the effective factors on watershed segmentation is the background noise which causes improper segmentation and results in the phenomenon of over-segmentation. Furthermore, in case of a low contrast image and its low gradient, the segmentation will face under-segmentation. This phenomenon makes the separate regions in the watershed image to be mixed with each other mistakenly. To avoid these phenomena and to segment the watershed image properly, the curvelet transformation has been used.

3.0 METHODOLOGY ON SAR IMAGES

The proposed method comprises several stages: in the first stage, the input SAR image is denoised; in the second stage, by applying the curvelet transformation on the denoised SAR image, the useful features are extracted to describe the texture. In the next stage, the labeling matrix is formed based on the extracted features, and finally, by applying a watershed transformation on the label matrix, the input SAR image texture is segmented and recognized. The block diagram of the proposed method is illustrated in Fig.5.

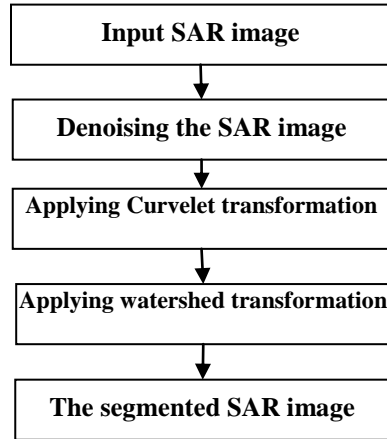


Fig. 5. Block diagram of the proposed method.

3.1 Denoising SAR Images

As SAR images are engaged with a noise phenomenon called speckle, the watershed transformation faces over-segmentation while segmenting the noisy images. Due to the excellent results from the Curvelet transformation in denoising SAR images, in this stage, the image noise is removed by applying Curvelet transformation on the main SAR image. Fig.6(a) illustrates the original image of a SAR image captured from Washington D.C. by a SAR satellite. The image is among the set of city images captured in X band. Fig.6(b) shows the noise removal of the image by the Curvelet transformation.

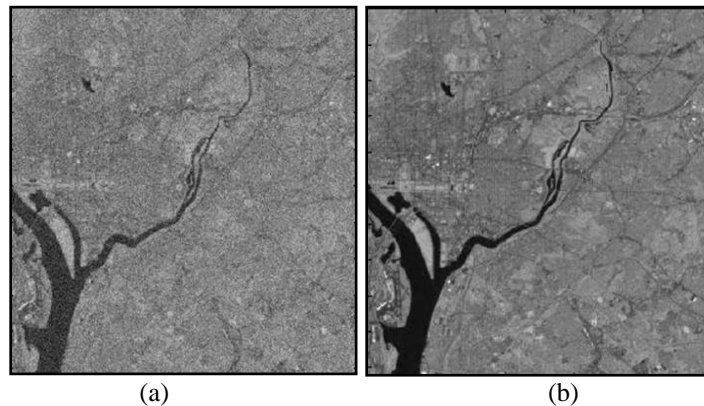


Fig. 6. (a) The original SAR image of a city region, and (b) Denoising SAR image of a city region by the Curvelet transform.

3.2 Image Location Decomposition

In this stage, the denoised SAR image is segmented into smaller blocks with no overlap. Although the image processing time is extended, the texture segmentation and recognition are done more carefully. In the present paper, the block size for each particular texture is 16×16 . The selection of SAR image blocks for each particular texture is

done through the selection of blocks with the optical images of the given region. Fig.7 illustrates an optical image of the same area of a city SAR image.



Fig. 7. Optical image of the same area with SAR image of a city region.

3.3 Describing Image Blocks

In this stage, the curvelet transformation describes the present information in the denoised SAR image blocks in the form of different sub-bands. Each sub-band of the transformation includes a certain level of degree and angle of separation. In the present paper, the curvelet transformation with the scale of 2 and angle of 8 is applied to the selected blocks, which leads to 9 sub-bands.

3.4 Feature Extraction

This stage plays a significant role in segmentation and recognition of SAR image textures. The selection features of this stage should be powerful enough so that different textures can be distinguished from one another. The feature extraction algorithm of each sub-band extracts the energy and the standard deviation of curvelet coefficients from the given sub-band. The reason for choosing the energy and standard deviation of curvelet coefficients as selected features is that their efficiency has been proved in a lot of past research [1, 2, 4, 15, and 45]. The features of energy and standard deviation of coefficients in different sub-bands are calculated and extracted respectively through the formulas as below:

$$E_i = \frac{1}{N_i} \sum_{j=1}^{N_i} |C_i(j)|^2. \quad (22)$$

$$STD_i = \sqrt{\frac{1}{N_i} \sum_{j=1}^{N_i} (|C_i(j)| - E_1)^2}. \quad (23)$$

In the formulas, i is the sub-band index, N_i is the number of the sub-band coefficients, and the parameter $C_i(j)$ is the j^{th} curvelet coefficient from the sub-band i .

3.5 Applying Watershed Transformation

As the obtained coefficients through curvelet transformation for various textures in a SAR image are different, the features of energy and standard deviation of different textures are different as well. To evaluate the performance of the proposed features, the moving and stationary target acquisition and recognition (MSTAR) public release data set is used [46]. The SAR images in the MSTAR data set have a resolution of $0.3 \text{ m} \times 0.3 \text{ m}$ with HH polarization by the Sandia National Laboratory X-band SAR sensor. The depression angles of the target images are 15° and 17° and that of the clutter images is only 15° . In this paper, 500 target images and 300 clutter scenes with 1784×1478 pixels are used. All these images, with a size of 128×128 , are distributed in the entire 360 azimuth coverage.

According to the proposed scheme, Tables 1 and 2 illustrate the extracted features from the first 4 sub-bands of curvelet transformation in some textures composed of water and vegetation regions in 800 SAR image. Note that the average of the results is presented in each section in these two tables.

Table 1. Extracted features for water region textures

Sub-band No.	1	2	3	4
Energy	1.3551e+003	0.0196	0.0257	0.615
Standard deviation	1.3184e+003	0.1246	0.1399	0.1993

Table 2. Extracted features for vegetation region textures

Sub-band No.	1	2	3	4
Energy	4.8899e+004	3.3353	3.8956	3.2249
Standard deviation	4.8678e+004	2.2874	2.7330	1.9670

By calculating watershed transformation, a labeling matrix is formed on the basis of the extracted features. In the given matrix, a single label is given to a certain texture in the image which represents watershed regions. Finally, by applying the watershed transformation on the whole matrix, the textures included in the image are classified and recognized.

4.0 EXPERIMENTAL RESULTS

To explain comparative advantages of the proposed algorithm with respect to LBF, wavelet model, and Gabor filter, the results of different algorithms on simulated and real SAR images are presented.

4.1 Segmentation and Classification of Simulated SAR Image

With the purpose of assessing the performance of the proposed method numerically, we first illustrate an experiment on a simulated three-look SAR image. This three-look simulated SAR image, as shown in Fig. 8(a), is produced by averaging three independent realizations of “Salt and pepper”, “Gaussian” and “speckle” noises. The ground truth image, as shown in Fig. 8(b), is used to compute the error rates of the segmentations and classifications obtained by different algorithms.

The four algorithms are used for segmentation and classification, respectively: 1) the LBF method [13]; 2) the wavelet transformation method [1]; 3) the Gabor filter method [47]; and finally 4) the proposed algorithm in this paper. Fig. 8(c) shows the segmentation result with the LBF model. Fig. 8(d) shows the recognition result of the wavelet, which is better than the LBF model. Fig. 8(e) shows the segmentation result obtained by the Gabor filter. Fig. 8(f) shows the best segmentation and classification result, according to the error rate. We found that the comprehensive error rates are reduced from 4.36% to 1.32% by using wavelet. The error rates have increased to 4.31% by using Gabor filter, and reduced to 1.29% by using the proposed algorithm. Therefore, Gabor filter is better than LBF, wavelet-based method is better than Gabor filter and the proposed algorithm outperforms the wavelet-based method.

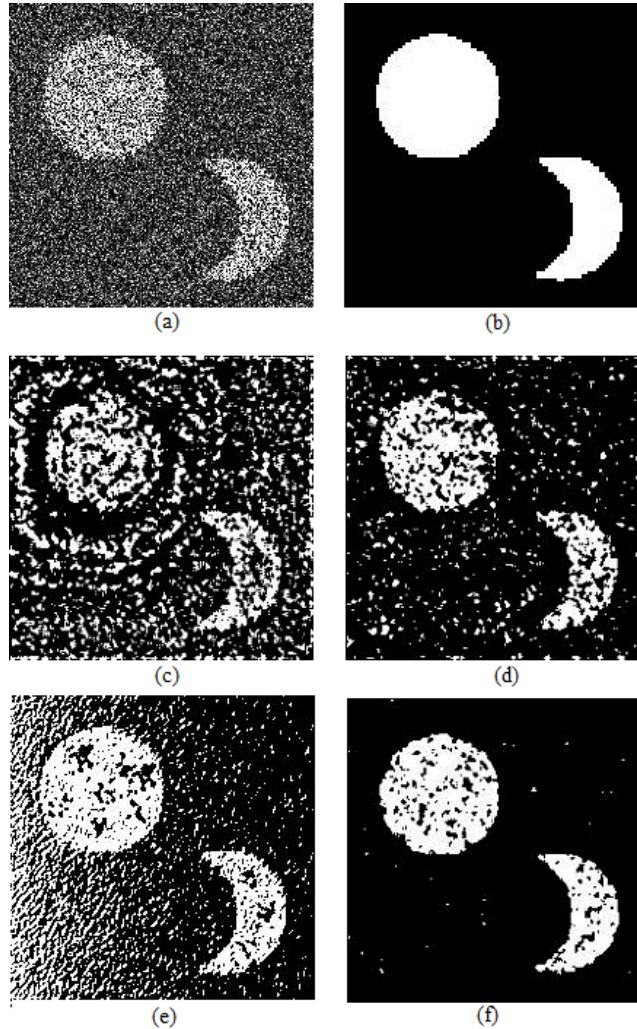


Fig. 8. (a) Three-look simulated SAR image (209×209), (b) ground truth, (c) segmentation obtained by LBF model[13] (error rate: 4.36%; the number of missegmented pixels: 1906), (d) recognition obtained by the wavelet transformation[1], (error rate: 1.32%; the number of missegmented pixels: 578), (e) segmentation obtained by Gabor filter[47](error rate: 4.31%; the number of missegmented pixels: 1883), and (f) recognition results obtained by the proposed method (error rate: 1.29%; the number of missegmented pixels: 564).

Visually, the segmentation of the LBF, which is shown in Fig. 8(c), is severely noisy in both uniform and non uniform regions. Many pixels in three segments are confused. The wavelet-based model performs better than the LBF, as shown in Fig. 8(d). The segmentation obtained by Gabor filter, which is shown in Fig. 8(e), is also spotty in both consistent and non consistent regions. Therefore, the wavelet-based model is more sturdy to the noise than the LBF and Gabor models. In the result, the missegmented pixels mainly locate in the black regions of Fig. 8(a), and the white regions of Fig. 8(a) are segmented better than the others. Compared with LBF, wavelet-based, and Gabor filter, the proposed method reduces the number of the missegmented pixels, as shown in Fig. 8(f).

4.2 Segmentation and Classification of Real SAR Images

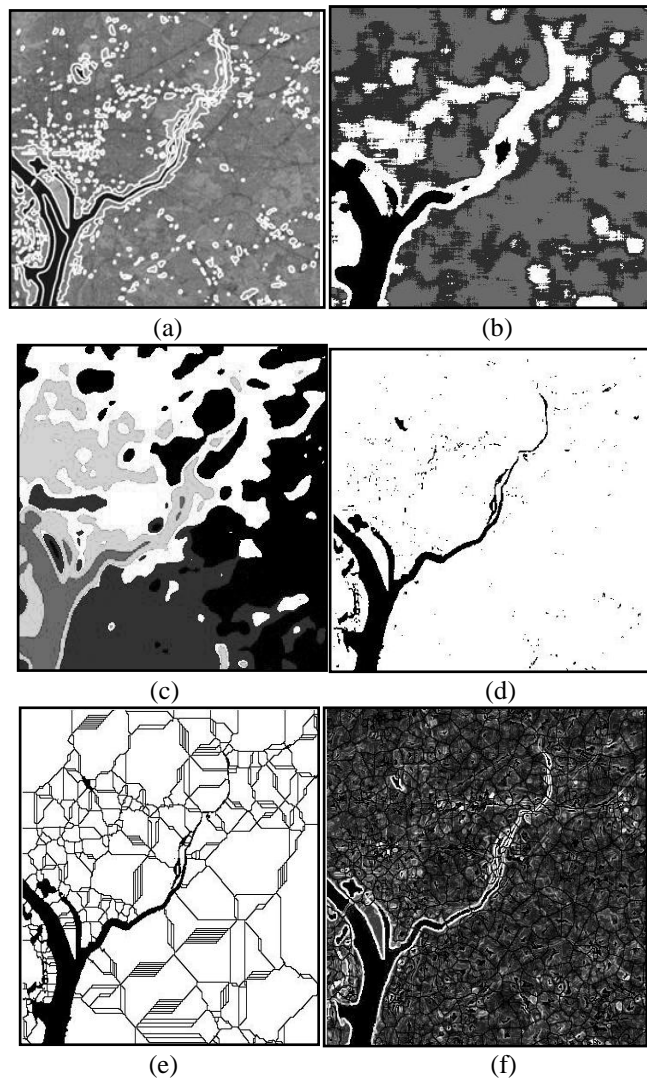


Fig. 9.(a) Segmentation results obtained by the LBF method [13], (b) recognition results obtained by the wavelet transformation[1], (c) segmentation results obtained by Gabor filter[47], and (d-f) recognition results obtained by the proposed method.

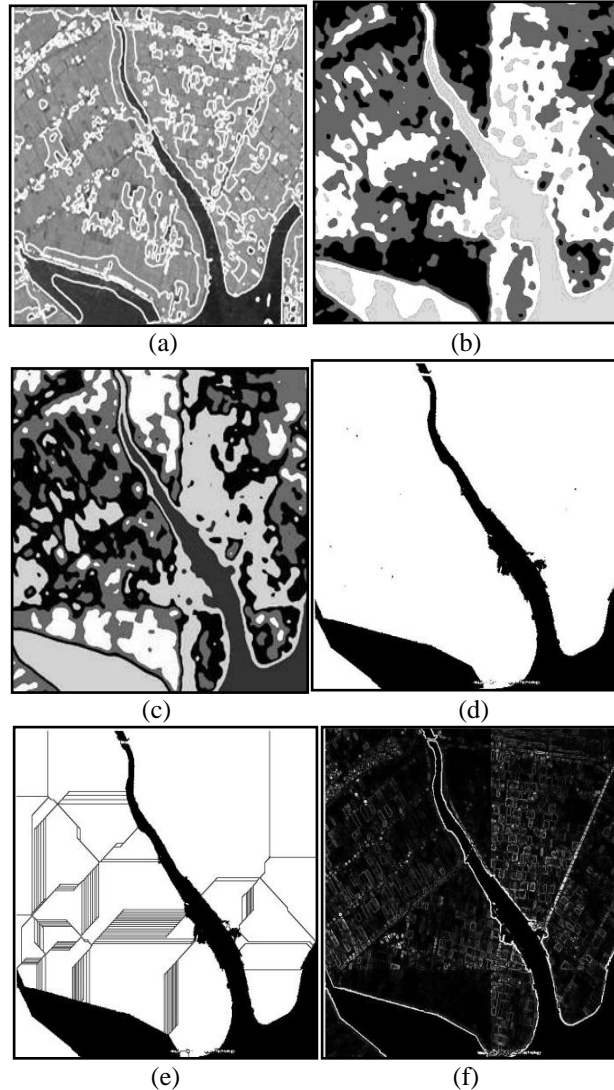


Fig. 10. (a) Segmentation results obtained by the LBF model [13], (b) recognition results obtained by the wavelet transformation [1], (c) segmentation results obtained by the Gabor filter [47], and (d-f) recognition results obtained by the proposed method.

In this subsection, the results on real SAR images will be discussed. The proposed method is applied to two different textures in the both mentioned images. One includes a city region, and another an agricultural area. Setting borders for water region and other ones in the image as well as the appearance of watershed lines are done by placing zero labels around the given label to the water regions in the labeling matrix. To do a comparison

between the results, the effects of the proposed method in the present paper have been compared with three sample methods, including LBF [13], wavelet transformation [1], and Gabor filter [47]. Fig. 9(a) illustrates the results from the LBF as a method based on the lightness intensity of pixels on water and vegetation covered regions. Fig. 9(b) illustrates the results from the tests of wavelet transformation for segmentation of the image. In this method, wavelet transformation and support vector machine have been utilized to recognize and segment the different textures. Fig. 9(c) illustrates the results from applying a Gabor filter for image segmentation. As it is shown, the water region textures have been improperly recognized and segmented. Furthermore, other texture has also been mixed and segmented wrongly. Fig. 9(d) to 9(f) illustrate the results of the experiments by utilizing the proposed method on the water region texture. The proposed method has improved the homogeneity of water regions so that the textures have been properly segmented in the three images. The proposed method can also be applied to other textures.

The next experiment has been carried out on a SAR image of an agricultural area. This image is taken of a rice-growing region near Okayama, Japan. It includes 5 different textures of water, buildings, plants, rice, and wheat. Results from LBF, wavelet transformation, and Gabor filter methods for image segmentation have been illustrated in Fig. 10(a) to 10(c) respectively. The water regions in this image have also been improperly recognized and segmented. The different textures in the images have been mixed and wrongly segmented. The segmentation and recognition results from the proposed method, as shown in Fig. 10(d) to 10(f), have better results over other methods. The border between water and other regions has been distinguished properly by watershed lines.

5.0 COMPARISON

Since the wavelet-based method proposed in [1] is better than LBF and Gabor filter methods, we would compare the ROC for the proposed method and the wavelet-based method [1]. The ROC of the mentioned two methods is shown as follows:

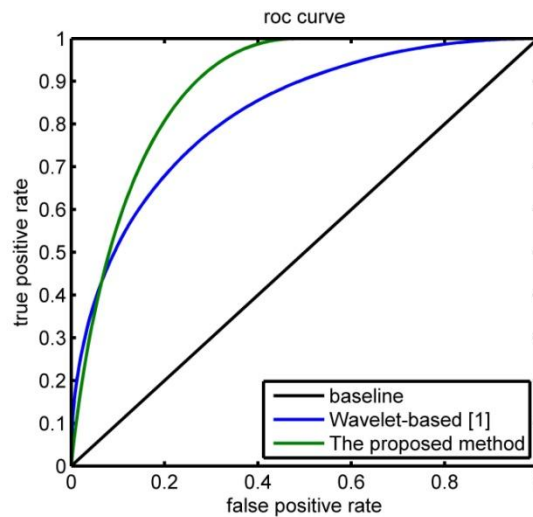


Fig. 11. The ROC curve of the wavelet transform and the proposed method.

As shown in the Fig. 11, the AUC of the proposed method is bigger than the AUC of wavelet-based method [1]. So, it can be concluded that, the accuracy of the proposed method is better than the wavelet-based method proposed in [1]. In the ROC curve, the x and y axis show the FPR and TPR respectively. As mentioned above, since the wavelet-based method is the best method of all three methods that has been compared to the proposed method, only the ROC curve in the proposed method and wavelet approaches, has been compared in this figure.

The area under the ROC curve is bigger in the proposed method. AUC [48] in the proposed method and wavelet is 0.86 and 0.83 respectively.

However, we can also compute the accuracy of the proposed algorithm without having any information about the ROC curve and compare it with other methods. As we know, since we have ground truth image, so we can calculate the number of white and black pixels. In this experiment, we have two errors:

- 1) The error of black pixels, which are classified incorrectly as white pixels.
 - 2) The error of white pixels, which are classified incorrectly as black pixels.
- To compute these two errors, we should compute the values below:
- a) The whole number of pixels in the image (**43681** pixels in our experiment).
 - b) The number of black pixels, which are classified incorrectly as white pixels (**452** pixels in our experiment).
 - c) The number of white pixels, which are classified incorrectly as black pixels (**112** pixels in our experiment).
 - d) The whole number of pixels with incorrect classification (b+c) which is **564** as reported in the experiment.
 - e) The whole number of pixels with correct classification (a-d), which is **43681-564 = 43117** pixels.

After computation of the black and white pixels in the ground truth image, these values are **35119** and **8562** for black and white pixels respectively. So, the error caused by black pixels is $\frac{452}{43681} = 0.0103$ and the error caused by

white pixels is $\frac{112}{43681} = 0.0026$. Thus,

The error of black pixels which are classified incorrectly as white pixels = 1.03%.

The error of white pixels which are classified incorrectly as black pixels = 0.26%.

The overall error rate is: 1.03% + 0.26% = 1.29%.

So, the accuracy is **98.71%**.

In the proposed method, if we consider the black pixels as positive, and the white pixels as negative, we have [48]:

Positive (P) = 35119, Negative (N) = 8562, True positive (TP) = 34667, and True negative (TN) = 8450. \Rightarrow Accuracy = 0.987,

which this accuracy is actually the normalized value of 98.71%, that we obtained previously for accuracy.

The accuracy in other methods is obtained in the same way. The accuracy in Gabor, LBF, and wavelet methods, are 95.69, 95.64, and 98.68 respectively.

6.0 CONCLUSION

Texture recognition in SAR images is very important and has many applications that can be implemented via segmentation. SAR images are of high resolution and can take images of various regions at any time of the day and in all weather conditions. However, due to the speckle noise, there are major problems in segmenting these images with common methods of image processing. This paper proposes a curvelet and watershed-based method for segmentation of SAR images and recognition of various textures in them. Curvelet is an effective method for noise reduction and extracting useful features. First, curvelet transformation is used for noise reduction. Curvelet reduces the noise without destroying the main information of the image. It preserves the edges and boundaries of the image

and does not blur them, which results in a more effective recognition of the information regarding the details of the SAR image. Next, 16×16 windows are extracted from various textures of vegetation and water. Since the energy and standard deviation of the curvelet coefficients are different in various sub-bands, these features play an important role in texture recognition of the radar images. Therefore, watershed transformation is applied on the image after feature extraction in order to segment it. The proposed method resolves the disadvantages of other methods to a desirable extent. As the results of the simulated and real images reveal, the presented method, which is proposed to recognize and study water and vegetation texture types, has a better performance compared to the other methods for both texture types. This is due to extracting more effective and better features in this method compared to the previous methods. Both visual and numerical comparisons indicate that the presented method is superior to the other methods, more powerful in segmentation, and has a better accuracy and lower segmentation error than these methods.

REFERENCES

- [1] G. Akbarizadeh, "A New statistical-Based Kurtosis Wavelet Energy Feature for Texture Recognition of SAR Images," *IEEE Transactions on Geoscience and Remote Sensing*, Vol. 50, No. 11, November 2012, pp. 4358-4368.
- [2] G. Akbarizadeh, "A New Recognition Approach Based on Genetic Algorithm for Classifying Textures in Satellite SAR Images," *International Journal of Remote Sensing Applications*, Vol. 2, No. 4, December 2012, pp. 7-19.
- [3] Vedavrath Lakide, "Classification of Synthetic Aperture Radar Images Using Particle Swarm Optimization Technique," *A thesis Submitted in Partial Fulfillment of the Requirements for the Degree of Master of Technology in Electronic Systems and Communications*, Reg. No: 207EE111, Department of Electrical Engineering, National Institute of Technology, Rourkela, 2009.
- [4] G. Akbarizadeh, "A New Kurtosis Wavelet Energy for Segmentation of SAR Images," *2nd National Conference on Soft Computing and Information Technology (NCSCIT 2012)*, Islamic Azad University of Mah shahr, March 8, 2012, pp. 312-315.
- [5] Z. Guangyi, Y. Cui, Y. Chen, J. Yin, J. Yang, and Y. Su, "Pol-SAR Images Classification Using Texture Features and the Complex Wishart Distribution," *IEEE Radar Conference*, May 2010, pp. 491-494.
- [6] K. Ersahin, I. G. Cumming, and R. K. Ward, "Segmentation and Classification of Polarimetric SAR Data Using Spectral Graph Partitioning," *IEEE Transactions on Geoscience and Remote Sensing*, Vol. 48, No. 1, January 2010, pp. 164-174.
- [7] M. S. H. Khiyal, A. Khan, and A. Bibi, "Modified Watershed Algorithm for Segmentation of 2D Images," *Issues in Informing Science and Information Technology*, Vol. 6, 2009, pp. 877-886.
- [8] K. Kayabol, and J. Zerubia, "Unsupervised Amplitude and Texture Classification of SAR Images with Multinomial Latent Model," *IEEE Transactions on Image Processing*, Vol. 22, No. 2, February 2013, pp. 561-572.
- [9] T. J. Kwon, J. Li, and A. Wong, "ETVOS: An Enhanced Total Variation Optimization Segmentation Approach for SAR Sea-Ice Image Segmentation," *IEEE Transactions on Geoscience and Remote Sensing*, Vol. 51, No. 2, February 2013, pp. 925-934.

- [10] P. Gamba, and M. Aldrichi, "SAR Data Classification of Urban Areas by Means of Segmentation Techniques and Ancillary Optical Data," *IEEE Journal of Selected Topics in Applied Earth Observations and Remote Sensing*, Vol. 5, No. 4, August 2012, pp. 1140-1148.
- [11] I. B. Ayed, A. Mitiche, and Z. Belhadj, "Multiregion Level-Set Partitioning of Synthetic Aperture Radar Images," *IEEE Transactions on Pattern Analysis and Machine Intelligence*, Vol. 27, No. 5, May 2005, pp. 793–800.
- [12] C. Li, C. Y. Kao, J. C. Gore, and Z. Ding, "Implicit Active Contours Driven by Local Binary Fitting Energy", *IEEE Conference on Computer Vision and Pattern Recognition (CVPR)*, June 2007, pp. 1-7.
- [13] C. Li, C. Y. Kao, J. C. Gore, and Z. Ding, "Minimization of Region- Scalable Fitting Energy for Image Segmentation", *IEEE Transactions on Image Processing*, Vol. 17, No. 10, October 2008, pp. 1940-1949.
- [14] C. Chesnaud, P. Refregier, and V. Boulet, "Statistical Region Snake-Based Segmentation Adapted to Different Physical Noise Models", *IEEE Transactions on Pattern Analysis and Machine Intelligence*, Vol. 27, No. 5, May 2005, pp. 793–800.
- [15] G. Akbarizadeh, Gh. R. Rad, and Sh. Baradaran, "A New region-Based active contour model with skewness wavelet energy for segmentation of SAR images," *IEICE Transactions on Information and Systems*, Vol. E93-D, No. 7, July 2010, pp. 1690-1699.
- [16] Y. Li, H. Gong, D. Feng, and Y. Zhang, "An Adaptive Method of Speckle Reduction and Feature Enhancement for SAR Images Based on Curvelet Transform and Particle Swarm Optimization," *IEEE Transactions on Geoscience and Remote Sensing*, vol. 49, no. 8, August 2011, pp.3105-3116.
- [17] E. J. Candès, L. Demanet, D. L. Donoho, and L. Ying, "Fast discrete curvelet transforms," *SIAM J. Multiscale Model. Simul.*, vol. 5, no. 3, 2006, pp. 861–899.
- [18] D. Chen and T. Xu, "Watershed Segmentation Using Curvelet and Morphological Filtering", *2nd International Congress on Image and Signal Processing, 2009. CISP '09, Tianjin*, pp.1-5, 17-19 Oct. 2009.
- [19] X. H. Yuan and B. P. Buckles, "Subband noise estimation for adaptive wavelet shrinkage," *Proceedings of the 17th International Conference on Pattern Recognition (ICPR 2004)*, vol. 4, 2004, pp. 858-888.
- [20] D. L. Donoho "De-noising by soft-thresholding," *IEEE Trans. on Information Theory*, vol. 41, 1995, pp. 613-627.
- [21] M. A. Shayegan, S. Aghabozorgi, and R. G. Raj, A Novel Two-Stage Spectrum-Based Approach for Dimensionality Reduction: A Case Study on the Recognition of Handwritten Numerals, *Journal of Applied Mathematics*, vol. 2014, Article ID 654787, 14 pages, 2014. doi:10.1155/2014/654787
- [22] E. J. Candès, and D. L. Donoho, "Recovering edges in ill-posed inverse problems: optimality of curvelet frames", *Annals of Statistics*, Vol. 30, No. 3, 2002, pp. 784-842.
- [23] J. L. Starck, E. Candès, and D. L. Donoho, "Astronomical Image Representation by the Curvelet Transform", *Astronomy and Astrophysics*, Vol. 398, No. 2, August 2003, pp. 785–800.
- [24] E. Candès and F. Guo, "New multiscale transforms, minimum total variation synthesis: Applications to edge-preserving image reconstruction," *Signal Process.*, vol. 82, no. 11, 2002, pp.1519–1543.

- [25] J. L. Starck, E. J. Candès, and D. L. Donoho, “The curvelet transform for image denoising,” *IEEE Transactions on Image Processing*, vol. 11, no. 6, 2002, pp.670–684.
- [26] E. J. Candès and D. L. Donoho, “Curvelets — a surprisingly effective nonadaptive representation for objects with edges,” in *Curve and Surface Fitting: Saint-Malo 99, 2000*. Cohen, C. Rabut, L. Schumaker. Vanderbilt University Press.
- [27] E. J. Candès and D. L. Donoho, “New tight frames of curvelets and optimal representations of objects with piecewise C^2 singularities,” *Communications on Pure and Applied Mathematics*, vol. 57, no. 2, Feb. 2004pp. 219-266.
- [28] J. Ma and G. Plonka, “Combined curvelet shrinkage and nonlinear anisotropic diffusion,” *IEEE Trans. Image Processing*, vol. 16, no. 9, pp. 2198–2206, 2007.
- [29] G. Plonka and J. Ma, “Nonlinear regularized reaction-diffusion filters for denoising of images with textures,” *IEEE Trans. Image Processing*, vol. 17, no. 8, 2008, pp. 1283–1294.
- [30] B. Zhang, J. Fadili, and J. Starck, “Wavelets, ridgelets, and curvelets for Poisson noise removal,” *IEEE Trans. Image Processing*, , vol. 17, no. 7, pp. 1093–1108, 2008.
- [31] L. Tessens, A. Pizurica, A. Alecu, A. Munteanu, and W. Philips, “Context adaptive image denoising through modeling of curvelet domain statistics,” *J. Electron. Imaging*, vol. 17, no. 3, 2008, pp. 03021:1–03021:17.
- [32] J. Ma, G. Plonka, “The curvelet transform,” *IEEE Signal Processing Magazine* , vol.27, n0.2, March 2010, pp.118-133.
- [33] HT. Nguyen and M. Worring, “Watersnakes: Energy-Driven Watershed Segmentation,” *IEEE Transaction on Pattern Analysis and Machine Intelligence*, vol. 25, no. 3, MARCH 2003, pp.330-342.
- [34] F. Meyer, “Topographic Distance and Watershed Lines,” *Signal Processing*, vol. 38, no. 1, July 1994, pp. 113-125.
- [35] G. Borgefors, “Distance Transforms in Digital Images,” *Computer Vision, Graphics, and Image Processing*, vol. 34, 1986, pp. 344-371.
- [36] S. Beucher and F. Meyer, “The Morphological Approach of Segmentation: The Watershed Transformation,” *Mathematical Morphology in Image Processing*, E. Dougherty, ed., chapter 12, 1992, pp. 43-481, New York: Marcel Dekker.
- [37] J. Serra, “Image Analysis and Mathematical Morphology”, 1982, *New York: Academic Press*.
- [38] F. Preteux, “On a Distance Function Approach for Gray-Level Mathematical Morphology,” *Mathematical Morphology in Image Processing*, E. Dougherty, ed., 1992, pp. 323-350, New York: Marcel Dekker.
- [39] C. Lantuéjoul, “ *La squelettisation et son application aux mesures topologiques de mosaïques polycristallines*,” *PhD thesis, Ecole sup'erieure des mines de Paris*, 1978.
- [40] C. Lantuéjoul and S. Beucher, “On the use of the geodesic metric in image analysis,” *Journal of Microscopy* vol. 121, no.1, 1981, pp.39-49.

- [41] F. Meyer, "The watershed concept and its use in segmentation: a brief history," arXiv preprint arXiv:1202.0216, February, 2012.
- [42] H. Digabel, C. Lantuejoul, "Iterative algorithms," In: *Proceedings of Quantitative Analysis of Microstructures in Material Science, Biology and Medicine. West Germany: Riederer Verlag, 1978, pp.85-99.*
- [43] S. Wang, X. Ma, X. Zhang, and L. Jiao, "Watershed-based textural image segmentation", International Symposium on Intelligent Signal Processing and Communication Systems, 2007. ISPACS 2007. Nov. 28-2007-Dec. 1 2007, pp.312-315.
- [44] M. Hamdi, "Modified Algorithm marker-controlled watershed transform for Image segmentation Based on Curvelet Threshold," *Middle-East Journal of Scientific Research*, vol. 20.no.3, 2014, pp.323-327.
- [45] J. F. Aujol, G. Aubert, and L. B. Feraud, "Wavelet-based level set evolution for classification of textured images", *IEEE Transactions on Image Processing*, Vol. 12, No. 12, December 2003, pp. 1634–1641.
- [46] <https://www.sdms.afrl.af.mil/>.
- [47] A. Teuner, O. Pichler, and B. J. Hosticka, "Unsupervised texture segmentation of images using tuned matched Gabor filters", *IEEE Transactions on Image Processing*, Vol. 4, No. 6, June 1995, pp. 863-870.
- [48] http://en.wikipedia.org/wiki/Receiver_operating_characteristic